Using KAF-4201 CCDs for astronomy

Anton Norup Sørensen
IJAF
Copenhagen University Observatory, Denmark
&
Dafydd Wyn Evans
Institute of Astronomy, Cambridge, UK

September 1999

1 Introduction

The work horse detector for cameras built at Copenhagen University Observatory has for several years been a Loral 2k by 2k, $15\mu m$ pixel CCD. The requirement for better spatial sampling in certain projects has forced us to look for alternatives to this detector. By now, two cameras have been built using the Kodak KAF-4201 CCD, with 2k by 2k, $9\mu m$ pixels. While this CCD fulfills our sampling requirements, trade-offs are made in other areas. In this presentation, the potential of the KAF-4201 as an astronomical imager is evaluated.

2 The Kodak KAF-4201 CCD

A short summary of the chip design: The detector has 2032 by 2044 imaging pixels, and a total of 2048 by 2048 pixels including dark current reference pixels. The pixels are $9\mu m$ square. The CCD is thick and front side illuminated, and has one output amplifier.

3 Cosmetics

A close inspection of the flat field uniformity is possible using images as those in figure 1. Here the CCD is uniformly illuminated through a 550nm narrow band filter. Apart from structures caused by vignetting, stray light and dust on the window, the sensitivity is strikingly uniform. About the only area with a diverging sensitivity is a small region, a 7 by 20 pixel area, where signal is about 30% lower than the surroundings, and a part of the missing charge is seen as a higher level in the neighbor pixels. In an attempt to identify bad pixels or columns, the ratio of a $80e^-$/pixel and a $57000e^-$/pixel flat field is examined. Traps and bad columns would appear as diverging numbers in the ratio image, but no such are seen.

A possible blemish is the presence of warm pixels. These are described in the section on dark current.

In all, the cosmetic quality of the detector is excellent, superior to all thinned, backside illuminated CCDs inspected at the observatory.

4 Charge Transfer Efficiency

4.1 Laboratory measurements

Examination of dark exposures in the laboratory immediately revealed a CTE problem, as can be seen in figure 2. Cosmic hits in the image are all displaying a vertical tail of deferred charge, indicating poor parallel CTE.

Our Fe-55 X-ray source could not easily be fitted onto the camera, so in stead another method was used for CTE characterization: The CCD has a relatively large number of hot pixels, that are spontaneously filling the pixel capacitor with charge during an integration. These are working as excellent point sources, as they do not suffer from charge diffusion and come in a wide range of intensities that can be further varied by changing exposure time and chip temperature. By measuring the strength of a tail from a hot pixel, the CTE can be determined as a function of both intensity and temperature.

The measured Charge Transfer Inefficiency (CTI = 1 - CTE) versus signal level is shown in figure 3. Measurements are shown for temperatures of $-60°C$, $-40°C$ and $-20°C$. At the highest temperature, the scatter in data points is severe due do cross-talk between the many dark pixels appearing at higher temperatures. At $-60°C$, there seems to be a simple relation between CTI and signal level, with an acceptable CTI of 10^{-5} at 10^4 electrons, but degrading to a very poor value of $8 \cdot 10^{-3}$ at 10^3 electrons. Going towards higher temperatures, the CTE is improving.

The CTE values mentioned above are for point sources on a zero level background. On our Schmidt telescope, looking at a light-polluted sky, the CTE problem is hard to notice. It seems that a sky background improves the CTE rapidly, to a higher degree that should be expected from figure 3.

4.2 CTE influence on astrometry

One of the cameras is installed on the Carlsberg Meridian Telescope on La Palma. The camera is used for making drift scan exposures of a large area on the sky. During analysis of the data, D. W. Evans found something wrong: Astrometry showed the faint stars to be shifted by up to half an arc second in right ascension relative to the bright stars. To test that the source for the error was bad CTE, he then examined the astrometry error's dependency on the background level due to varying moon phases, and found a nice correlation. In figure 4, the position error versus star magnitude is plotted for high and low background levels. The offset can be nicely described as a function of star and background magnitude, and the error can be corrected. But of course, a better solution would be to improve the detector CTE. It will now be tried to run the detector at a higher temperature, where CTE is expected to be better and the dark current has not yet risen to an unacceptable level.

5 RON, linearity and full-well

The read-out noise was measured to 7 e^- for a read-out speed of 60Kpix/sec, significantly below the factory specifications of 15 e^- at 1Mpix/sec. Unfortunately, due to the low level CTE problem, the signal quality is very poor at the level where RON is of importance.

A quite precise measurement of linearity is reached by simply measuring the ADU level versus exposure time, using a stable light source. Measurements made in this way are plotted in figure 5. The response is seen to be linear to within $\pm 1\%$ for the middle illumination range and up to the full well limit. For low counts, below about $2000e^-$/pixel, there seems to be a considerable deviation from linearity. This will pose a serious problem to photometry of faint objects. It remains to be determined whether the linearity deviation is linked to the CTE problem, but as the linearity was determined from flat field exposures and not images of point sources, one would not immediately expect a connection.

The full well is determined as the highest illumination level where the gain measured from the noise statistics does not deviate from it's semi-constant level. In this way, the full well is found to be $120Ke^-$.

The appearance of saturated stars can be studied in figure 6. The brightest star displays blooming along the parallel register, but stars not quite so bright show a horizontal tail. This is believed to be due to a surface full well in the horizontal register being lower than the full well in the parallel register. The surface full well reveals itself by the characteristic poor high level CTE.

6 Quantum-efficiency

A QE plot for 11 narrow bands is shown in figure 7. The sensitivity is at a level of about 35% from 550nm to 770nm. Longwards of this, QE drops relatively slowly due to the large thickness of the CCD. At short wavelengths the sensitivity drops off rapidly, as is typical of front-side illuminated CCDs, and no significant flux is detected shortwards of 405nm. The measured QE is generally slightly lower than the product specifications. The sensitivity found is in all as expected for a thick, front side illuminated CCD. The stability of the sensitivity seems excellent, as no change was noted during the test period.

7 Dark current

The KAF-4201 CCD is designed to have a low dark current even at ambient temperature. In this application, the CCD is cooled, and the dark current should then be very small. The amount of dark current has been determined from a series of 1800 sec dark exposures with a detector temperature of approximately -60°C. The level was found to be 5 electrons/pixel/hour.

A median-clipped image of six 1200 sec dark frames is shown in figure 8. Several hot pixels are present, with intensities of up to about 10.000 e^-/hour. These are affected by the poor CTE and display vertical tails.

The on-chip amplifier circuit emits light onto the array, which can be seen in the lower left corner of the figure. With the voltages required for read-out, the intensity of the light is quite high. Because of this, the output drain voltage is lowered during integration, which reduces the light emission to a neglectable level for most applications.

8 Modulation Transfer Function

The ability of the detector to spatially sample an image is not only determined by the pixel size, but also by internal charge diffusion. As we earlier had experienced detectors with considerable charge diffusion that severely limited spatial resolution, this point was of particular interest.

Data for measurement of the Modulation Transfer Function have been collected by measuring the contrast of fringes of different spatial wavelengths projected onto the CCD. The illumination wavelength was 670nm, which has a relatively small absorption depth. As the CCD is front-side illuminated, the MTF is expected to be very good for short wavelength illumination. Analysis of the data revealed MTF variations in periodic patterns on the surface of the CCD. This is attributed to interference between the fringes and the front side electrodes. Only illumination with a wide slit gave reasonable results, probably because this attenuated the interference. The results are shown in figure 9. Curves for the pixel geometry MTF and slit MTF are shown. Note that the very wide slit strongly affects the directly measured result. Data are plotted for the raw measurements, and plotted after these measurements are corrected for pixel geometry and slit width. The last curve thereby represents the intrinsic MTF of the Silicon. After the corrections, a very high MTF is measured, compared to previous measurements of thinned back-side illuminated CCDs. The intrinsic curve seems to flatten or even increase slightly at high frequencies, which is most likely a too optimistic result.

In all, the detector with it's small $9\mu m$ pixels and small charge diffusion, fulfills our requirement for good spatial sampling.

9 Conclusion

The KAF-4201 detector fulfills our expectations in the area that was the primary reason for selecting it: It has excellent spatial resolution. The cosmetic quality is near perfect, and RON and QE are acceptable and as expected for the design type.

Unfortunately the low level CTE is found to be very poor and also the response deviates strongly from linearity at low levels. The quality of scientific data from the cameras are severely affected by this.

We have been operating the two cameras built with the detectors cooled to -60°C. As the CTE is expected to improve with higher temperature and the dark current is relatively low at high temperatures, we will try to use a higher detector temperature to see if this improves the quality of the data.

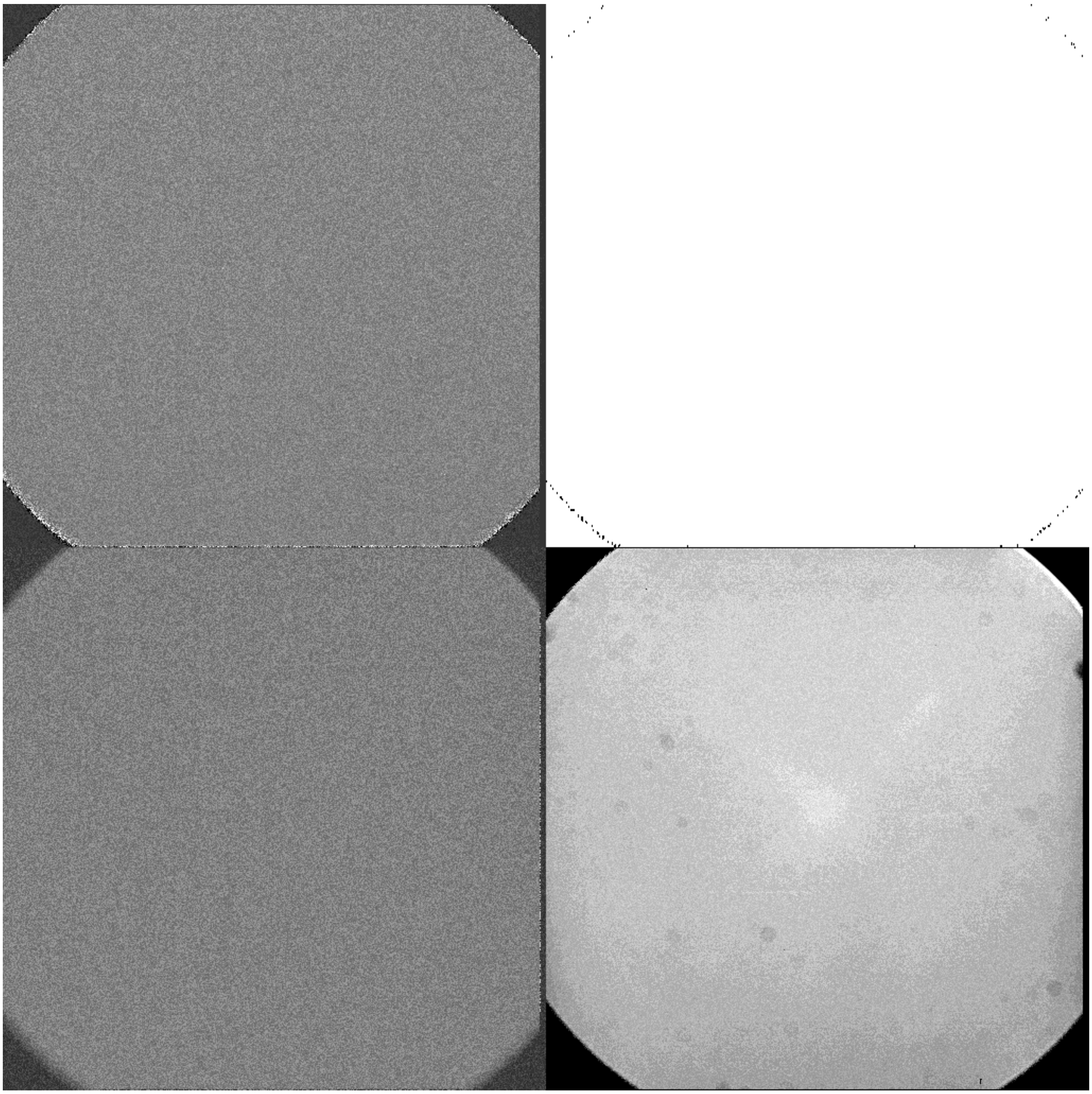

Figure 1: Comparison of a 550nm high and low illumination flat field, in order to identify charge traps. *Lower left:* Flat field at an illumination level of $80e^{-}$/pixel. Grey scale cuts are ± 300% of median level. *Lower right:* Flat field at an illumination level of $57.000e^{-}$/pixel. Grey scale cuts are ± 8% of median level. *Upper left:* Ratio of the two flat fields. Bright lines should appear where charge is lost in the low level flat field, and vice versa, but no bad pixels or columns are seen. Grey scale cuts are ± 300% of median level. *Upper right:* Map of deviating points in the ratio image - only vignetting is causing a few points.

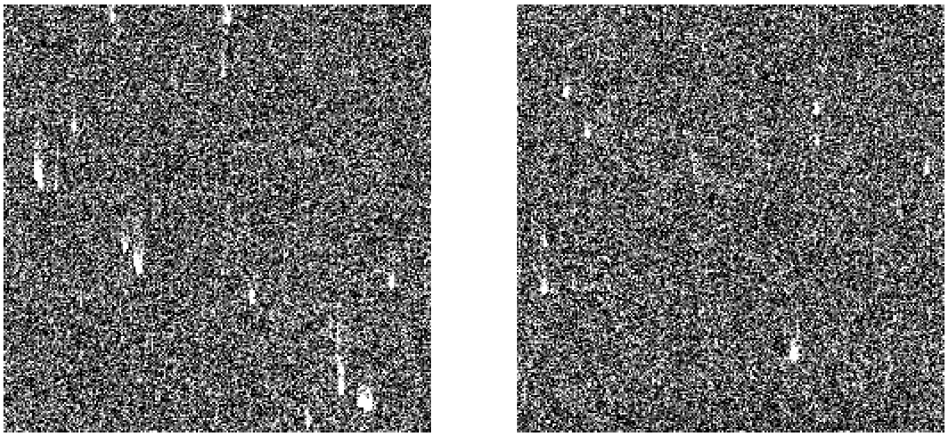

Figure 2: Sections of a dark frame with several cosmic hits. Left: Top of image, furthest away from the serial register. Cosmics show strong tails. Right: Bottom of image, just outside the serial register. Cosmics have faint tails.

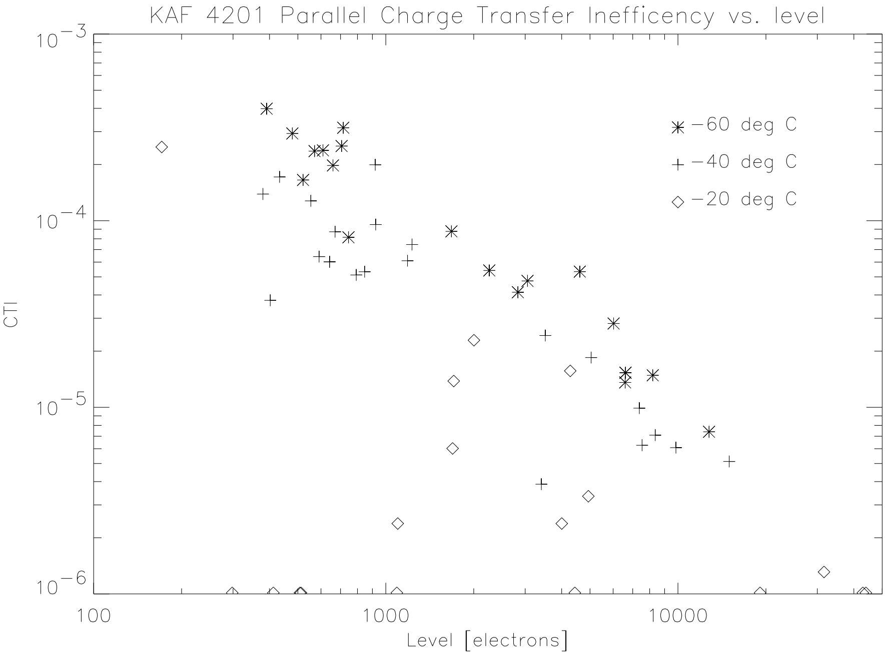

Figure 3: Charge Transfer Inefficiency measured from warm pixels of different intensity. The CTI is strongly depending on signal level: Acceptable CTI is found at high signal levels, but a very poor value at low signal levels. The measurements are made at three different temperatures, indicating improving CTE with higher temperature.

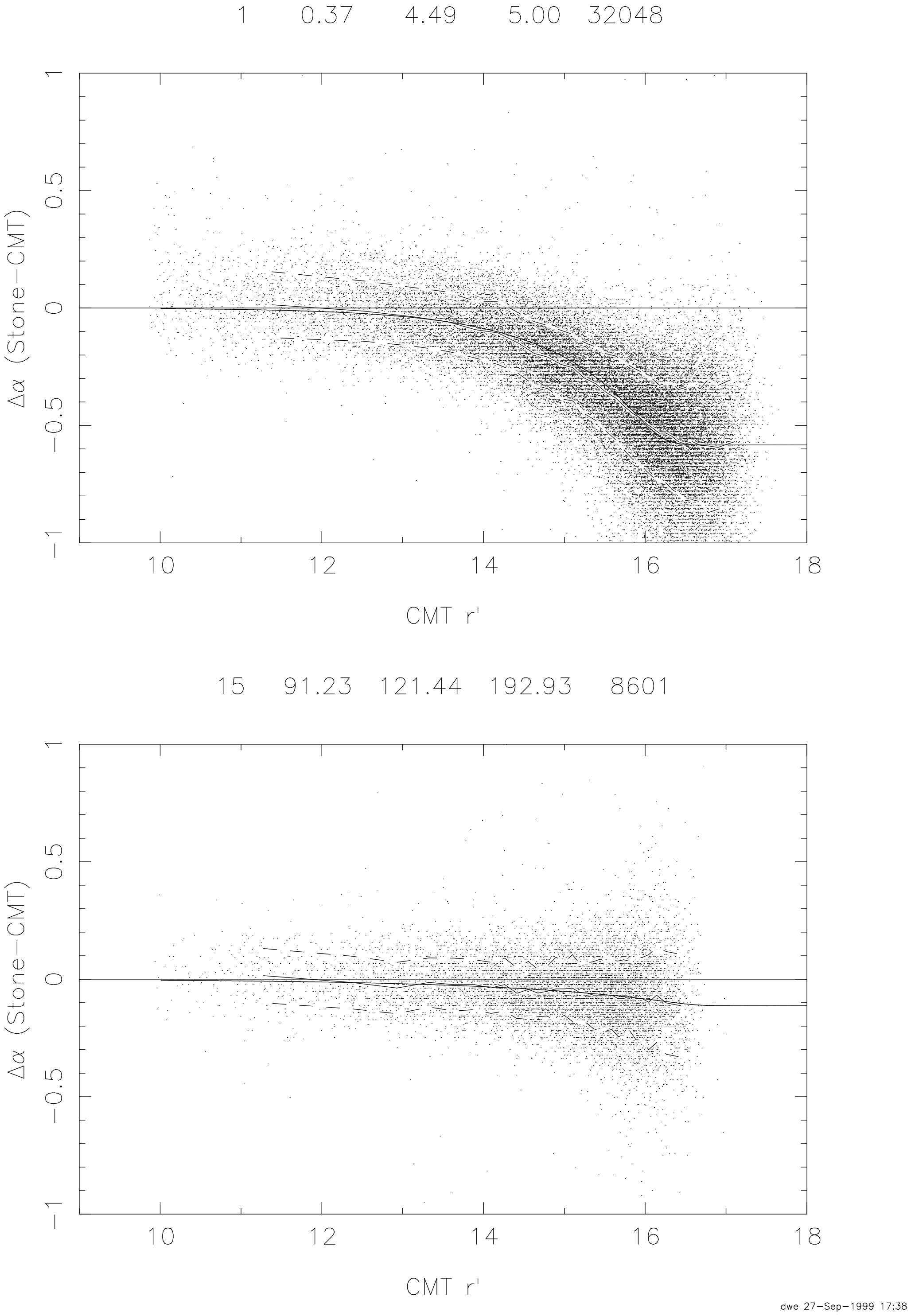

Figure 4: Plots showing the discrepancy in right ascension position between CCD frames and catalogue coordinates. The deviation increases for fainter magnitudes, reaching about 0.5 arcsecond at the limiting magnitude. The upper graph shows measurements for a dark sky, while the lower is for a strongly Moon-lit sky. As the background increases, the position error gets smaller because of better CTE at higher signal levels.

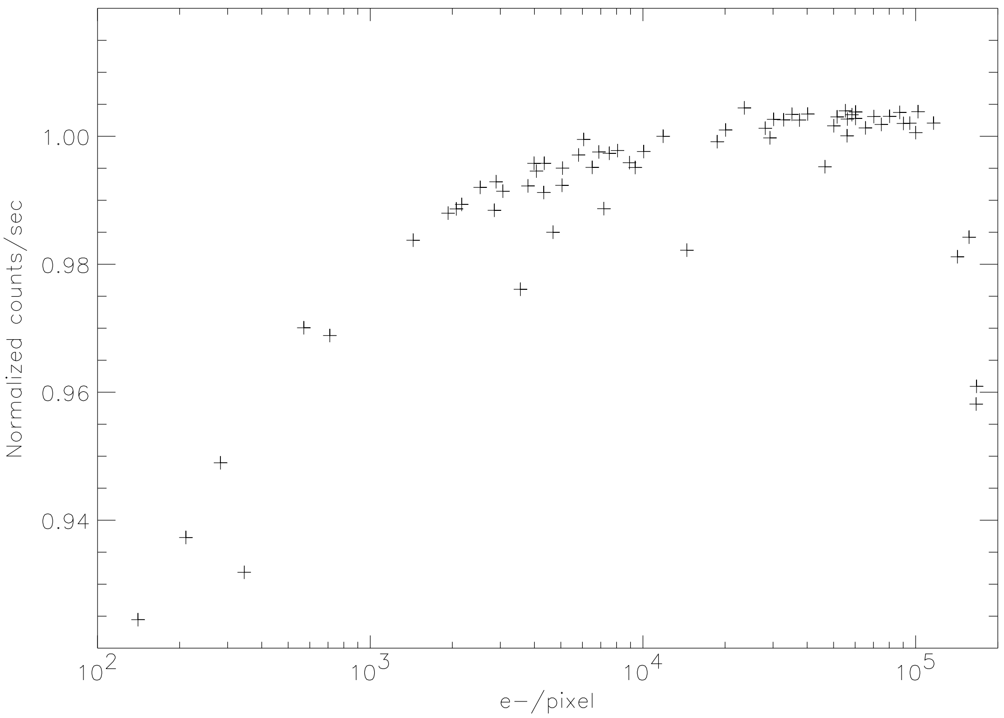

Figure 5: A plot of the registered counts per second of exposure, using various exposure times. With a stable light source and shutter delay correction applied, this describes the linearity of the detector response. A strong linearity deviation is seen below approx. 2000 e^-. Above $120Ke^-$ signal drops due to saturation.

Figure 6: 240 sec B, V, R exposures combined to a color picture of the Dumbbell nebula. Due to a bright sky background, the faint stars do not appear affected by low level CTE problems. The brightest stars are smeared in the horizontal direction, because of a low surface full well in the serial register. One star also shows normal blooming along the parallel register. Recorded using the Brorfelde Schmidt telescope by Karl Augustesen, CUO. Processed by Søren Larsen, CUO.

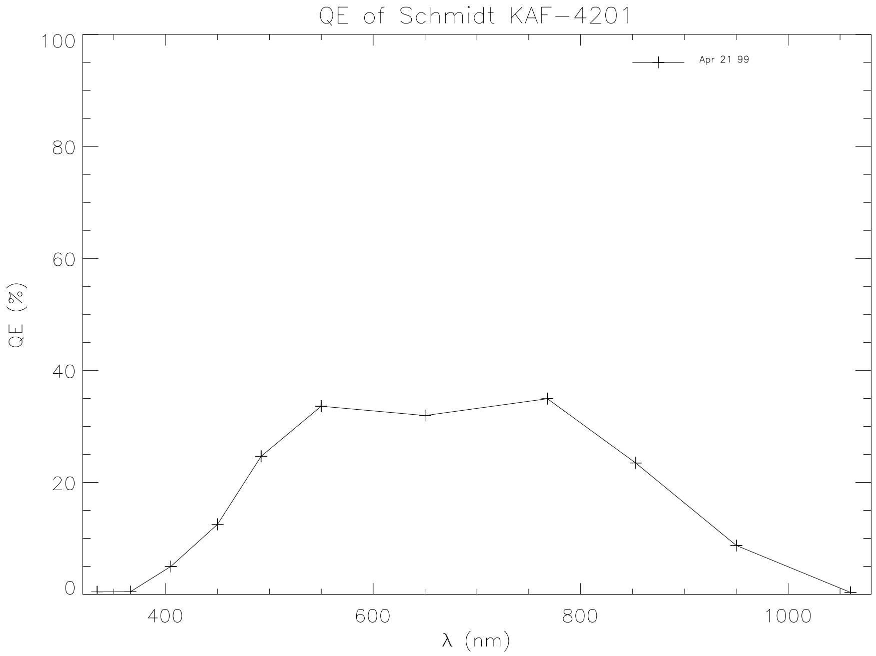

Figure 7: Global quantum efficiency versus wavelength for the KAF-4201 CCD, measured from the sigma-clipped mean of the central area of a flat field exposure.

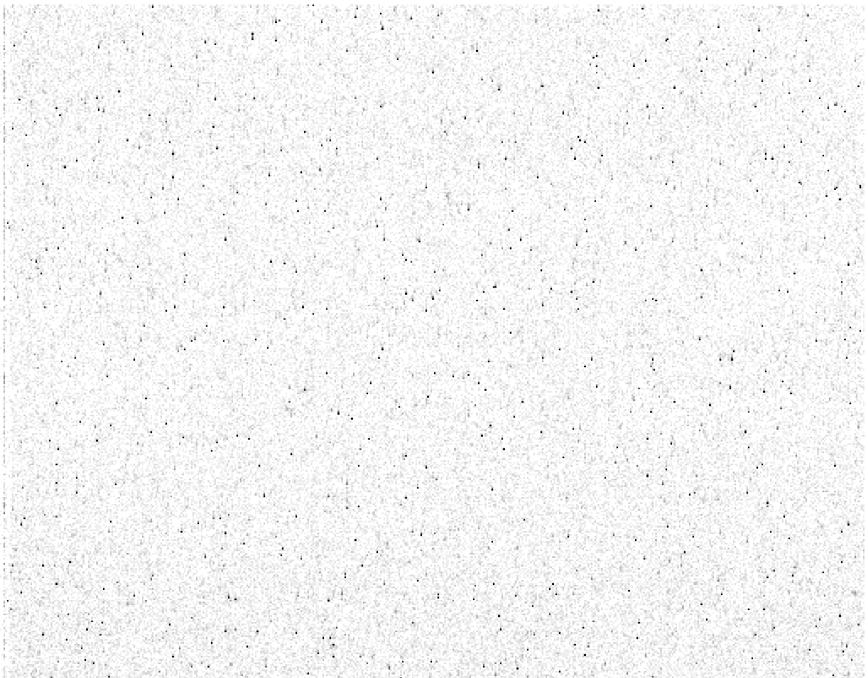

Figure 8: A median image of six 1800 sec dark exposures, made with a detector temperature of -60°C. The grey scale is inverse, with values above 20 ADU drawn as black. The overall structure is flat, but there are several hot pixels. In one corner, the luminisence of the on-chip amplifier is seen even though the voltages to the amplifier are reduced during the integration.

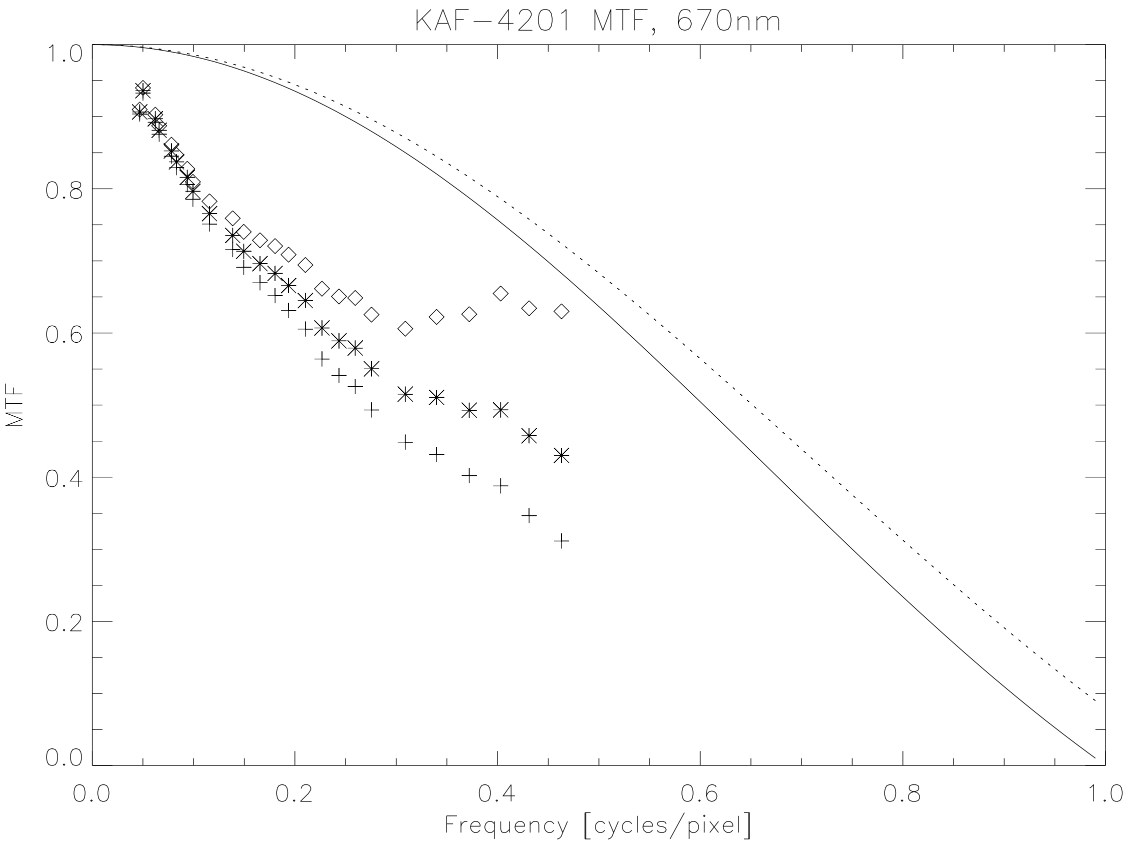

Figure 9: Measured Modulation Transfer Function for the KAF-4201 CCD. Solid line: MTF of the box-car pixel geometry. Dashed line: MTF of the illumination slit. Crosses: Measured MTF without corrections. Asterixes: MTF corrected for pixel geometry. Diamonds: MTF corrected for pixel and slit geometry, i.e. the MTF of the Silicon alone.